High-temperature fiber-optic lever microphone

Allan J. Zuckerwar
NASA Langley Research Center, Hampton, Virginia 23681

Frank W. Cuomo
F. W. Cuomo Consulting Services, East Providence, Rhode Island 02914

Trung D. Nguyen
Old Dominion University, Norfolk, Virginia 23508

Stephen A. Rizzi and Sherman A. Clevenson
NASA Langley Research Center, Hampton, Virginia 23681

(Received 13 September 1994; accepted for publication 3 February 1995)

The design and construction of a fiber-optic lever microphone, capable of operating continuously at temperatures up to 538 °C (1000 °F), are described. The design is based on the theoretical sensitivities of each of the microphone system components, namely, a cartridge containing a stretched membrane, an optical fiber probe, and an optoelectronic amplifier. Laboratory calibrations include the pistonphone sensitivity and harmonic distortion at ambient temperature, and frequency response, background noise, and optical power transmission at both ambient and elevated temperatures. A field test in the Thermal Acoustic Fatigue Apparatus at Langley Research Center, in which the microphone was subjected to overall sound-pressure levels in the range of 130–160 dB and at temperatures from ambient to 538 °C, revealed good agreement with a standard probe microphone.

PACS numbers: 43.38.Kb, 43.38.Zp, 43.58.Vb

INTRODUCTION

The measurement of pressure fluctuations in hypersonic flow fields imposes severe demands upon a measurement microphone, which must be capable of operating at the high temperatures usually associated with high-speed boundary layers (e.g., 1093 °C or 2000 °F), at the high frequencies associated with flow instabilities, and at the high acoustic intensities associated with separating flows and shock/boundary layer interaction. Further, a small microphone size is desirable not only to obtain a high-frequency response but also to reduce spatial averaging errors due to the finite size of the active element. Among the requirements are typically a temperature rating of 1093 °C, continuous service; a frequency bandwidth of 25 or 100 kHz, depending on application; and a dynamic range of 130–190 dB, *re*: 20 μPa. The available technologies capable of producing a microphone to satisfy these, especially the high-temperature requirement, are limited.

A major difficulty with microphones utilizing constitutive properties of materials—like piezoelectricity, piezoresistivity, or magnetostriction—is that no known materials exhibit these properties at 1093 °C, and even at low temperatures they require compensation for their temperature dependence.[1,2] Further, these materials present practical problems at elevated temperatures like lead attachment.

The eddy current probe of Kaman Sciences[3] has proved operable at temperatures up to and exceeding 1093 °C. However, a small button, where the eddy currents are generated, is attached to the vibrating membrane and thus severely limits the frequency response of the microphone. At present this technology may not permit a frequency response as high as 100 kHz.

Interferometric fiber-optic sensors of the Mach–Zehnder, Michelson, or Fabry–Perot types perform well within the controlled confines of the laboratory.[4] However, in hostile field environments, their performance degrades due to their sensitivity to vibration and thermal gradients (changes in wavelength) along the entire length of the fibers. Furthermore, many of these sensors contain critical optical components in locations that would be exposed to the high service temperatures.

The condenser microphone, being a high impedance device, requires a preamplifier in close proximity to the microphone cartridge to suppress electromagnetic interference and loading by cable capacitance.[5] The preamplifier cannot withstand the high-temperature environment.

The use of pressure ports and probe tubes not only limits the high-frequency response but also induces distortion of the output signal due to acoustical wave interference and damping.[6]

The practice of water cooling conventional microphones is not practical for flight testing.

Thus it is concluded that state-of-the-art technology is incapable of fulfilling the requirements of hypersonic testing.

The technology selected to achieve the required specifications is based on the principle of the fiber-optic lever.[7] Here light reflected from a stretched membrane is intensity-modulated by the motion of the membrane, which is excited by incident sound. The optical fiber serves as a conduit for light transmission to and from the membrane. As in the condenser microphone, the transduction is a purely geometric effect, which promotes stability at elevated temperatures.

 0001-4966/95/97(6)/3605/12/$6.00

The use of an optical fiber for the transmission of the acoustical data permits remote placement of the signal conditioning electronics (away from the hot zone) and provides immunity from electromagnetic interference.

Since an effort to develop a microphone to operate at 1093 °C was deemed too great a leap from ambient temperature, it was decided to proceed in two steps: first, to develop a 538 °C (1000 °F) microphone, and then, based on this experience, a 1093 °C microphone. The choice of 538 °C as the intermediate temperature is based on the availability of conventional materials for the microphone cartridge and of optical fibers rated for this temperature. A 1093 °C microphone cartridge, utilizing platinum alloys, has been fabricated, but comparably rated optical fibers (e.g., sapphire or inconel coated silica) require further development.

The fiber-optic lever microphone (FOLM) system consists of a microphone cartridge, an optical fiber probe, and an optoelectronic amplifier. Consequently, the microphone system sensitivity M_S is the product of the three component sensitivities:

$$M_S = M_M M_O M_E . \tag{1}$$

In Eq. (1) the mechanical sensitivity M_M is the membrane displacement per unit incident sound pressure in m/Pa, the optical sensitivity M_O is the change in optical power per unit membrane displacement in W/m, and the electrical sensitivity M_E is the output voltage per unit change in optical power in V/W.

The purpose of this paper is to describe the 538 °C FOLM system: the construction, design, and theoretical sensitivity of each of the components listed above, a discussion of background noise sources (Secs. I–III), laboratory calibration at ambient and elevated temperatures (Sec. IV), and finally, the results of a field test in a high-temperature, high-acoustic-intensity environment (Sec. V).

I. THE MICROPHONE CARTRIDGE

A. Construction

Figure 1 shows a photograph and cross-sectional view of the cartridge. The cartridge parts fulfill three primary functions: securing the membrane, adjusting the membrane tension, and gripping the optical fiber probe.

The membrane is made of 25.4-μm (0.001 in.) thick nickel 200 foil. A disk is cut out of the foil, polished to a high reflectance on one side, coated with a 0.5-μm layer of quartz, and formed into the shape of a cup. After the latter is placed over the tension ring and body, it is secured in place by means of a press-fitted weld ring. In order to avoid relying on friction to retain the membrane under tension, the membrane, weld ring, and body are electron-beam welded together.

The tension ring is hemispherically contoured to insure contact with the membrane at all times, especially during the rarefaction half-cycle at high sound pressures. The hole in the center determines the diameter of the active membrane, which can be as small as the optical fiber probe or nearly as large as the tension ring itself.

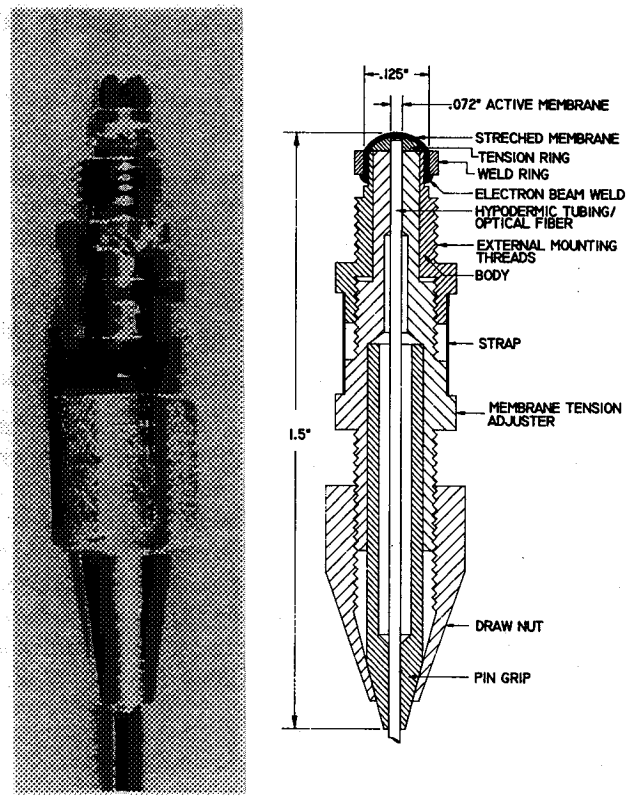

FIG. 1. Photograph and cross-sectional view of the microphone cartridge.

The tension adjuster, when torqued relative to the body, advances along the cartridge axis, exerts pressure on the tension ring, and applies tension to the membrane. The membrane tension is controlled, with good reproducibility, by the torque reading on a torque screw driver, which is fitted with a socket adapter to engage a hex nut on the body. After the torque adjustment is completed, two straps are spot-welded between the body and adjuster nuts to prevent changes in adjuster position.

The pin vise assembly consists of a pin grip to hold the optical fiber probe in place and a draw nut to exert pressure on the pin grip. Further detail is given in Sec. II.

In addition, the cartridge incorporates external threads for installation in a panel. The cartridge does not contain a backplate to dampen the membrane motion, however, because the path from the optical fiber to the membrane mirror must remain optically transparent. Neither does it contain a capillary vent for static pressure equalization on the interior side of the membrane, a function assumed by leakage through the optical fiber probe.

B. Design

The high-temperature requirement makes the membrane design fundamentally different from that of a conventional ambient temperature microphone. The three leading effects of high temperatures on microphone performance must be accounted for.

(1) A reduction in membrane tension: Because the stretched membrane represents approximately a constant strain system, the temperature dependence

of the tension follows that of the elastic modulus. Since the modulus of nickel 200 falls by 21% between 20 and 538 °C,[8] one might expect a concomitant rise in sensitivity and drop in resonance frequency. However, as will be shown in Sec. IV, the actual membrane behavior is to the contrary—an effect believed due to the presence of the protective quartz layer.

(2) Thermal expansion: The primary influence is a change in the position of the fiber relative to the membrane mirror. If the fiber position is optimized at ambient temperature, then a change in fiber position will reduce the microphone sensitivity.

(3) An increase in air viscosity: Since this is important only near the membrane resonance, it plays no role in the membrane design. Neither does the decrease in air density, since the compliance is completely controlled by the membrane tension.

The membrane design is based on the following expressions for the membrane resonance frequency f_R,[9] mechanical sensitivity M_M,[10] and tension T:

$$f_R=\frac{2.4048}{2\pi a}\left(\frac{\sigma_{rr}}{\rho_M}\right)^{1/2}, \tag{2}$$

$$M_M=a^2/(4T), \tag{3}$$

$$T=\sigma_{rr}t, \tag{4}$$

where a is the membrane radius, t the thickness, ρ_M the density, and σ_{rr} the radial stress. Two choices were made *ab initio*. First, the membrane thickness was chosen to be 25.4 μm (0.001 in.), at least 5× thicker than that of commercial microphones, for additional ruggedness is needed for a harsh high-temperature, high-intensity environment. Second, the stress σ_{rr} is designed not to exceed the yield stress at 538 °C (88 MPa at 0.2% elongation[8]) in an effort to insure a recoverable modulus with temperature cycling. It was found empirically that a torque setting of 12 in.-oz on the tension adjuster provides the required tension in the membrane. Then, given a density $\rho_M=8900$ kg/m^3, a value of $a=9.144\times10^{-4}$ m (0.036 in.) inserted into Eq. (2) yields a membrane resonance frequency of 41.6 kHz, adequate to insure the desired bandwidth of 25 kHz. The minimum practical value of $a=4.064\times10^{-4}$ m (0.016 in.), limited by the radius of the optical fiber probe, yields a resonance frequency very close to 100 kHz. The protective quartz layer, however, stiffens the membrane and causes the measured resonance frequencies to exceed the design values.

Table I summarizes the pertinent cartridge properties at 20 and 538 °C. The depth of the hole in the tension ring (below the active membrane) is 7.87×10^{-4} m (0.031 in.) at ambient temperature. For optimal sensitivity the optical fiber probe protrudes through the hole a distance of typically 2.87×10^{-4} m, leaving a fiber–membrane gap of 5.00×10^{-4} m. The adjacent region is considered to be a slot, for which the dimensions are listed in the table. Of course, the back-chamber volume is zero. Figure 2 shows the corresponding theoretical frequency response curves according to the theory presented in Ref. 10. The predicted response is highly underdamped because of the absence of a backplate, a feature

TABLE I. Microphone and air properties at ambient and elevated temperatures.

Property	Units	20 °C (68 °F)	538 °C (1000 °F)	Multiply by
Membrane				
radius	m	9.144	9.216	10^{-4}
thickness	m	2.54	2.56	10^{-5}
density	kg/m^3	8900	8688	···
tension	N/m	2722	2235	···
sound speed	m/s	109.7	100.2	···
Air layer				
gap	m	5	5.04	10^{-4}
density	kg/m^3	1.205	0.435	···
viscosity	Ns/m^2	1.79	3.68	10^{-5}
specific-heat ratio	···	1.403	1.353	···
isothermal sound speed	m/s	289.9	482.5	···
Slot				
location	m	6.60	6.66	10^{-4}
width	m	5.08	5.13	10^{-4}
depth	m	2.87	2.90	10^{-4}

which admits compensation through electronic filtering. The predicted rise in sensitivity and loss of bandwidth at high temperature are also apparent. Comparison with experiment will be discussed in Sec. IV.

The above choice of design parameters is consistent with the specification on the upper limit to the dynamic range. The maximum shear strain in a stretched membrane due to a uniform incident pressure p_i is easily found to be[10]

$$\epsilon_{\eta r}=\frac{\partial\eta}{\partial r}=\frac{p_i a}{(2T)},$$

which exceeds the radial strain ϵ_{rr} by orders of magnitude. With the parameter values listed in Table I for 538 °C, an incident pressure $p_i=6.32\times10^4$ Pa (190 dB SPL) will produce a maximum shear strain $\epsilon_{\eta r}=1.3\%$, which is sufficiently small to result in negligible harmonic distortion (see Sec. IV A).

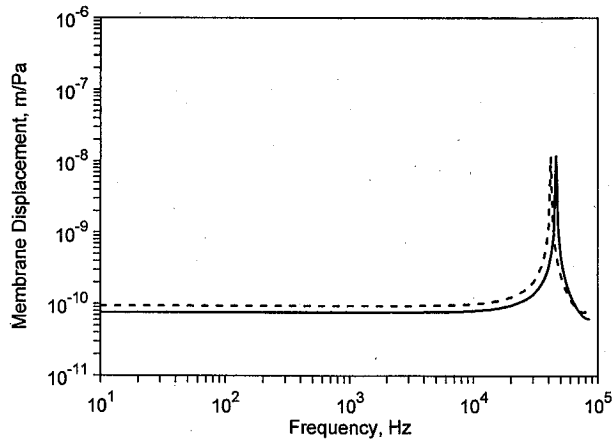

FIG. 2. Theoretical frequency response of the membrane displacement at ambient temperature (solid line) and 538 °C (dashed line). The fundamental resonance frequencies are 45.930 and 41.631 kHz, respectively.

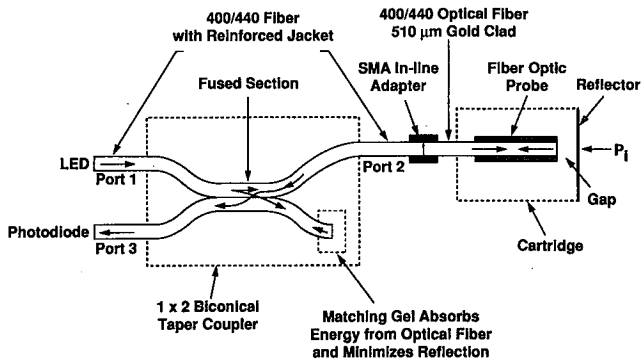

FIG. 3. Schematic diagram of the optical system for the single fiber optical probe.

II. THE OPTICAL FIBER PROBE

A. Construction

Two optical fiber lever arrangements can be used to construct the probe for the detection of axial pressures acting on a reflector. The first, identified as the multifiber probe, features a construction consisting of several multimode step-index fibers arranged in a bundle at the distal end.[11] The second arrangement utilizes an optical coupler to permit a single fiber to transmit the light to a reflector, while the modulated return signal is fed back into the same optical fiber for processing. Both methods have been investigated, and both multifiber and single fiber probes have been fabricated and tested at ambient and high temperatures reaching 538 °C with good results. However, one drawback with the multifiber arrangement has been the inability to establish stable conditions after several thermal cycles. This instability has been attributed to changes in the position of the optical fibers at the distal end after heating. For this reason the single fiber approach was chosen for further investigation and becomes the major topic of discussion in this paper.

The arrangement used for the single fiber probe is shown in Fig. 3. The basic components consist of a cartridge, a fiber-optic probe, a fiber-optic coupler, and optoelectronic transmitting and receiving units. Details of the single fiber optic probe are given in Fig. 4. It includes a probe tip constructed to accommodate the 400-μm core, gold coated, multimode, step-index optical fiber used in our experiments. The optical fiber is secured to the probe tip by introducing a ceramic adhesive suitable for high-temperature operation, as shown in Fig. 4. Ceramic cement Aremco type 569 was found to be satisfactory for our application. To prevent microcracks from developing at high temperatures in the silica glass, the optical fiber is protected by an outer gold coating.

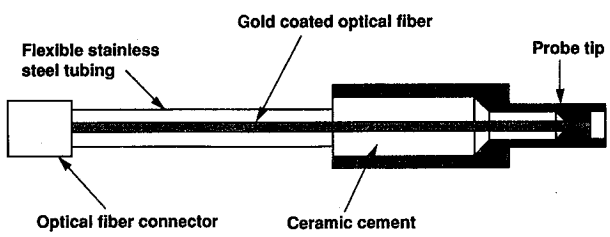

FIG. 4. Details of the single fiber optical probe.

Optical fiber type AF400/440G procured from Fiberguide Industries is used. The temperature range suggested by the manufacturer is from −190 (−310 °F) to 750 °C (1382 °F). The end of the fiber in the probe tip is polished for best results with lapping paper as fine as 0.3-μm grit. The other end of the optical fiber is cemented into an optical fiber connector, Amphenol SMA series 905/906, and the fiber length (typically 1 m) between the connector and the probe tip is protected with flexible stainless-steel tubing, Flextron F-ISS steel square locked flexible tubing.

Multimode fiber-optic couplers, as shown in Fig. 3, were procured from Tacan Corp., Carlsbad, CA. The fiber cores at the fused section were adjusted for a coupling ratio of 50%. The optical fibers identified as port 1 and port 3 in Fig. 3 are connected to an optoelectronic transmitting unit and receiving unit, respectively, as described in Sec. III.

The general operation of the electro-optical device in Fig. 3 begins with a light source which couples into an optical fiber. One half of the light bypasses the fused section of the coupler and exits through the other end of the coupler (port 2). The end of this fiber is connected to an Amphenol SMA connector and coupled to the fiber-optic probe via an Amphenol SMA adapter. The light enters the cartridge where it is reflected by the reflective element, which is modulated by the external field. The modulated reflected light follows the same path back to the fused section of the coupler where 50% of the light enters the second fiber, continues to port 3, and eventually impinges on the photodiode in the receiving unit. It is noted that the other half of the light entering port 1 couples into the second fiber at the fused section. To avoid unwanted reflections from the fiber end, this energy is absorbed by the matching gel, as shown.

To complete the fabrication of the high-temperature microphone, the polished end of the optical fiber probe is inserted into the cartridge and the gap is adjusted at room temperature for maximum response. This setting is performed with a micrometer adjustment while the assembled cartridge is installed in a high-pressure microphone calibrator, Bruel & Kjær type 4221. The adjustment is made while the calibrator is driven at a frequency of 1000 Hz. Upon completion of the gap adjustment, the probe tip of the fiber-optic probe, shown in Fig. 4, is held in place by tightening the draw nut unto the pin grip, shown in Fig. 1, and bonded with the high-temperature cement.

B. Design

The theoretical and experimental analyses of the single and multifiber microphones have been evaluated. The results for the multifiber microphone have been described previously.[10,11] In brief, the theoretical approach in both designs assumes that the input fiber is illuminated by a Lambertian source, such as a light emitting diode. This implies that the incident light rays will couple the same amount of optical power into the optical fiber core of the transmitting fiber independent of the incident angle up to the cutoff angle, which is determined by the numerical aperture. Figure 5 illustrates the basic concept for the single fiber design. A light source illuminating the transmitting fiber will contain beams arriving from all angles θ with respect to the fiber axis and

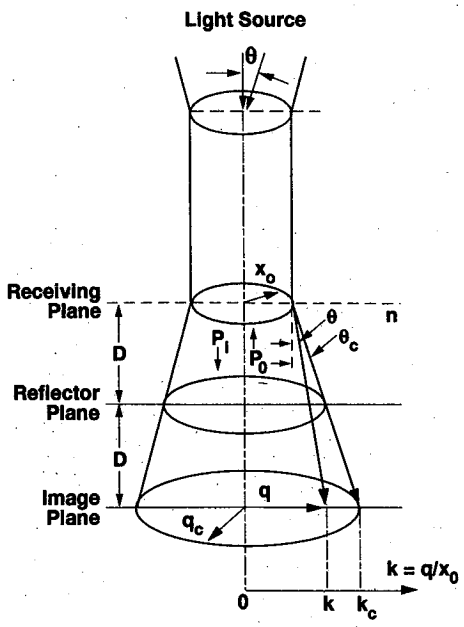

FIG. 5. Coordinates of the single fiber fiber-optic lever.

the rays limited by $\theta \leqslant \theta_c$ will couple into the fiber. Here θ_c is the cutoff angle determined by the numerical aperture and the refractive index n of the surrounding medium. Similarly, the light rays exiting the distal end will form a cone with a maximum angle θ_c. The beam in the direction between θ and $+d\theta$ is defined as a uniangular beam for $0 \leqslant \theta \leqslant \theta_c$ and the reflected intensity of the receiving plane is equivalent to that on the image plane. Define $k = q/x_o$ as a dimensionless coordinate on the image plane, while $k_c = q_c/x_o = 1 + (2D/x_o)\tan(\theta_c)$ gives the boundary of the illuminated area; x_o is the fiber core radius, q the variable radius on the image plane, and q_c its boundary; k and θ are related by $\theta = \tan^{-1}[(k-1)x_o/(2D)]$; P_i is the total optical power exiting the transmitting fiber and P_o is the power reflected back into the same fiber. Further details of this approach have been given elsewhere.[11]

The acousto-optical parameters used in the evaluation of the two approaches are based on the behavior of the optical power delivered to the photodetector upon reflection from the membrane installed in the microphone cartridge. These parameters are defined for the single fiber according to Fig. 5. The optical transfer function P_o/P_i represents the normalized optical power as a function of the gap D. This expression for the multifiber lever is given by Eq. (16) in Ref. 11, while for the single fiber design, the transfer function P_o/P_i is revised to account for reflection into the transmitting fiber:

$$\frac{P_o}{P_i} = 2\int_0^1 I_k' k \, dk, \tag{5}$$

where I_k' is the normalized light intensity function described in Ref. 11.

The expressions defining the reflected optical power change Γ, the modulation index Q, and the shot-noise limited detectable threshold ΔD are, respectively,[7,12]

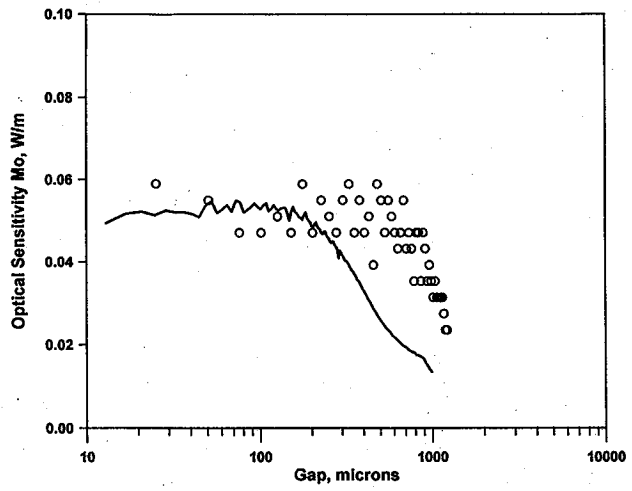

FIG. 6. Optical sensitivity M_O vs mirror–fiber gap D. Theoretical [Eq. (9)]: solid line. Experimental: symbols.

$$\Gamma = \frac{d}{dD}\frac{P_o}{P_i} \, (\mathrm{m}^{-1}), \tag{6}$$

$$Q = \frac{1}{P_t}\frac{dP_t}{dD} \, (\mathrm{m}^{-1}), \tag{7}$$

$$\Delta D = \frac{1}{Q}\left(\frac{2eB}{\rho P_t}\right)^{1/2} (\mathrm{m}). \tag{8}$$

In Eqs. (7) and (8) P_t is the total optical power reaching the photodetector ($=0.5\ P_o$ for a 50/50 coupler), ρ is the detector responsivity in A/W, e is the electronic charge in C, and B is the detection bandwidth in Hz. The remaining quantities are identified in Fig. 5. Equations (6)–(8) apply to both the multifiber and single fiber designs. The normalized modulation index Q is an important quantity because it can be used to determine the performance of any optical fiber sensor. This quantity is derived from the transfer function and the reflected optical power change. From the modulation index Q, the shot-noise limited detectable threshold ΔD is determined. The optical sensitivity M_O, defined in Eq. (1) as the change in optical power per unit membrane displacement, can be predicted theoretically as

$$M_O = -QP_t(\mathrm{W/m}). \tag{9}$$

C. Results

Optical power measurements were obtained for the single fiber sensor. The distal end of a fiber probe, consisting of a single 400/440-μm fiber, was installed in a microphone cartridge and a translational micrometer device was used to allow minute changes in the gap D. The other end of the probe was connected to port 2 of the optical fiber coupler, shown in Fig. 3, while the optical power from port 3 was monitored by a Newport model 815 power meter. A light emitting diode type 1A208, supplied by ABB-HAFO, was connected to port 1 of the coupler. With this experimental arrangement it was possible to monitor the optical power reaching the photodiode as a function of the gap D. Figure 6 yields the theoretical and experimental data illustrating the behavior of the optical sensitivity M_O. The theoretical re-

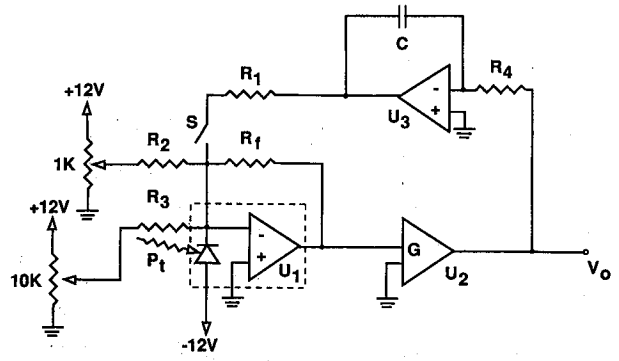

FIG. 7. Schematic diagram of the photodetector circuit. Legend: $R_1=10$ K, $R_2=15$ K, $R_3=200$ K, $R_4=1$ M, $R_f=10$ K, $C=0.1$ μF, U_1=EG&G HFD 1060, U_2=AD524, U_3=OP27.

sults were derived from Eq. (9), while the experimental measurements were obtained from the setup described above. The scatter reflects the limited resolution of the micrometer (± 1 μm). To obtain the theoretical results, a typical measured value of 224 μW for light coupled into the transmitting fiber ($2P_i$) was used. In order to account for losses incurred in the measurements, the theoretical data were reduced by a factor of 0.8×0.25. This included a factor of 0.8 due to reflection losses at the mirror, while the losses due to the coupler and optical fiber connections were estimated at 0.25. Comparison between the theory and experiment indicates very consistent results. It is noted that a flat response for gaps up to 200 μm is evident. Thus it is possible to install the distal end of the probe very close to the reflector to improve the membrane damping.[10] A delayed roll-off for the experimental data is also noted. This effect can be attributed to extraneous reflections occurring within the cartridge walls. However, no attempt has been made to account for this deviation from theory.

From the optical power measurements, the optical power P_t reaching the photodetector was found to be 70 μW at a gap D of 107 μm. Based on a detector responsivity ρ of 0.6 A/W and a 1-Hz bandwidth B, Eqs. (6)–(9) yield a reflected optical power change $\Gamma=1230\ \mathrm{m}^{-1}$ (@ $D=107$ μm), modulation index $Q=-1400\ \mathrm{m}^{-1}$, and detectable threshold $\Delta D=5.6\times 10^{-11}\ \mathrm{m}/\sqrt{\mathrm{Hz}}$.

It is important to note, however, in agreement with Fig. 6, that the signal output during calibration was found to remain fairly constant for gaps ranging from 100 to 800 μm. For this reason the operating gap was chosen somewhere between 300 and 600 μm to reduce the changes in sensitivity after several thermal cycles due to expansion or contraction of the optical fiber at the distal end.

III. THE OPTOELECTRONIC AMPLIFIER

A. Construction

The optoelectronic amplifier incorporates a light emitting diode (LED) driver circuit, a photodetector circuit, an output amplifier, and an optical coupler (for the single fiber probe). See Fig. 7.

The LED is a GaAlAs ABB-HAFO type 1A208, having a peak spectral output between 790 and 850 nm. The LED is built directly into an SMA receptacle. According to our own measurements the optical power coupled into a 400-μm fiber is roughly 400 μW.

The photodetector circuit converts an optical input signal at the photodiode to an electrical output signal. The photodiode is a silicon EG&G HFD 1060, having an active area of 1.5 mm^2 and, with a built-in OP AMP U_1, a peak responsivity of typically $\rho=0.6$ A/W at 900 nm. It is biased at -12 V to establish a photoresistive mode of operation.

Amplifier U_2, an AD524 instrumentation amplifier, provides a gain $G=100$, as adjusted for full-scale output at a 190-dB input sound-pressure level (SPL).

The output offset voltage V_{odc} can be nulled manually, with switch S open, by means of the 1-K (coarse) and 10-K (fine) adjustable resistors. When switch S is closed, the offset is nulled automatically by means of integrating OP AMP U_3. In this mode the amplifier becomes a high-pass filter with a time constant

$$\tau=R_1R_4C/GR_f.$$

With the values shown in the caption of Fig. 7 the time constant is 0.01 s, corresponding to a lower cutoff frequency of 17 Hz.

The electrical sensitivity of the FOLM system over the passband is found to be

$$M_E=V_0/P_t=\rho R_fG. \tag{10}$$

TABLE II. Theoretical and experimental noise power spectral densities in V^2/Hz at ambient and elevated temperatures (referred to the output V_0).

Theoretical noise source	Eq.	20 °C (68 °F)	538 °C (1000 °F)	Multiply by
Mechanical Johnson,[a] R_A	(7a)	0.396	2.106	10^{-26}
Shot: Dark[b]	(7b)	0.992	0.992	10^{-12}
Membrane radiation[c]	(7b)	0.054	0.186	10^{-12}
LED[c]	(7b)	2.732	2.056	10^{-12}
Electrical Johnson, R_f	(7c)	1.617	1.617	10^{-12}
Electrical Johnson, R_1, R_2, R_3	(7d)	2.787	2.787	10^{-12}
Total noise, theory		8.182	7.638	10^{-12}
Total noise, experiment		10.175	9.571	10^{-12}

[a] $R_A=1.2\times 10^5$ Ns/m^5 at 20 °C and 2.3×10^5 Ns/m^5 at 538 °C, derived from the theoretical frequency response computation shown in Fig. 2.
[b] Measured dark current $I_D=3.1$ μA.
[c] Responsivity $\rho=0.58$ A/W. Optical power into photodiode=14.72 μW at 20 °C and 11.08 μW at 538 °C (microphone H15).

B. Background noise

The "background noise" of a microphone is defined as the rms output in the absence of acoustical excitation. It is one of the most important microphone specifications, for it determines the minimum detectable SPL. Table II summarizes the principal sources of background noise in the FOLM system. The power spectral density J_n of the total background noise at the output is the sum of the contributions J_i from each source:

$$J_n=\sum_i J_i=\sum_i \frac{V_{oi}^2}{\Delta f},\quad i=1,2,\ldots . \tag{11}$$

The principal contributions referred to the output V_o are

(1) *mechanical Johnson noise*, due to the discreteness of the air molecules impinging upon the membrane,[10]

$$J_1 = 4K\Theta R_A M_S^2; \tag{12a}$$

(2) *shot noise in the photodiode*, originating from the dark current I_D and currents due to illuminating optical power sources, P_t from the LED and P_M the blackbody radiation from the membrane mirror,[13]

$$J_2 = 2eR_f^2 G^2 (I_D + \rho P_t + \rho P_M); \tag{12b}$$

(3) *electrical Johnson noise* in the feedback resistor R_f,

$$J_3 = 4K\Theta R_f G^2; \tag{12c}$$

(4) *electrical Johnson noise* in the bias and offset resistors R_1, R_2, and R_3,

$$J_4 = 4K\Theta R_f^2 G^2 (1/R_1 + 1/R_2 + 1/R_3). \tag{12d}$$

In Eqs. (11) and (12) Δf is the frequency resolution, R_A the membrane damping resistance, K the Boltzmann constant, and Θ the absolute temperature. Less significant noise sources, such as blackbody noise generated within the optical fibers, Johnson noise generated in the photoresistor, and $1/f$ noise, will be neglected. The $1/f$ noise, however, was found to be significant at elevated temperatures (see Sec. V). All the sources considered have a uniform power spectral density ("white" noise) over the operating bandwidth of the microphone.

Equations (9) and (12b) reveal that the microphone signal-to-noise ratio at the optoelectronic amplifier output increases monotonically with the optical power P_t incident upon the photodiode. It increases linearly with P_t at low P_t and as $\sqrt{P_t}$ at high P_t. In any case it is advantageous to couple as much light as possible from the LED into the optical fiber.

Table II compares the theoretical and experimental (see Sec. IV C) noise power spectral densities. The dominant contributions are the shot noise due to the LED illumination and the Johnson noise in the bias and offset resistors. An increase in optical power, although increasing the shot noise, will improve the signal-to-noise ratio since it increases the signal at a faster rate. A substantial reduction in the electrical Johnson noise offers a potential improvement of about 3 dB in the background noise and microphone sensitivity.

C. Overall microphone sensitivity

Equations (3), (9), and (10) and parameter values taken from Tables I and II permit the component sensitivities to be computed. The results for M_M, M_O, and M_E are 7.68×10^{-11} m/Pa, 0.0399 W/m, and 6×10^5 V/W, respectively. From Eq. (1) the theoretical microphone sensitivity is then $M_S = 1.84$ μV/Pa. This is compared to the pistonphone calibration of microphone H18 prior to the first exposure to high temperature, for this is the condition corresponding most closely to the values in the tables. The pistonphone calibration yielded $M_S = 1.43$ μV/Pa, in excellent agreement with the above. The measured value for the received light was $P_t = 28.51$ μW, which was used to compute M_O in Eq. (9).

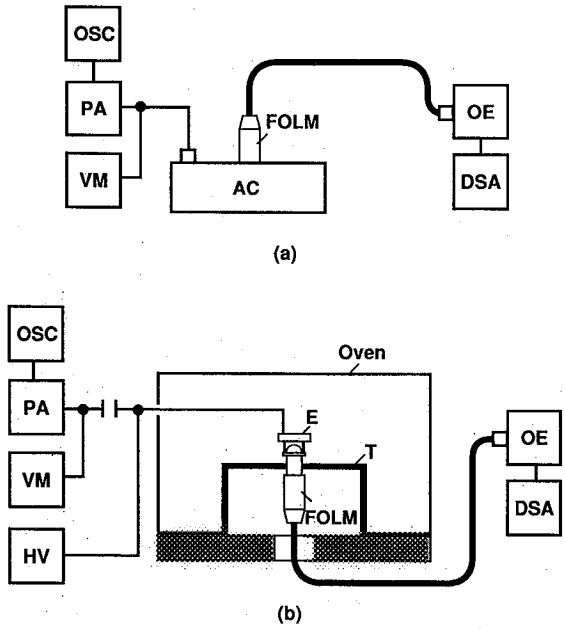

FIG. 8. Block diagram for (a) pistonphone calibrations and (b) electrostatic actuator calibrations. Legend: OSC=oscillator, Lorch Adret model Codasyn 201; PA=power amplifier, B&K type 2713; VM=voltmeter, HP 3403C; OE=optoelectronic amplifier, in-house; DSA=digital signal analyzer, B&K type 2032 (up to 25.6 kHz) or PC based system (>25.6 kHz); AC=acoustic calibrator, Whittaker model PC-125; HV=high-voltage supply, in-house; E=electrostatic actuator electrode; T=table; FOLM=fiber-optic lever microphone.

IV. LABORATORY CALIBRATION

Laboratory calibrations of the microphones were based on measurements with the following apparatus: a pistonphone, to measure absolute sensitivity and harmonic distortion, an electrostatic actuator, to measure frequency response and microphone stability with temperature cycling, and an optical power meter, to measure optical transmission through the fibers. The electrostatic actuator setup was also used to measure the background noise. The pistonphone measurements were conducted at ambient temperature only, the remaining measurements at both ambient and elevated temperatures. Examples of all the measurements will be illustrated, except as noted, for a selected prototype microphone H18.

A. Pistonphone calibration

The setup for the pistonphone calibrations is shown in Fig. 8(a). The pistonphone, a Whittaker PC-125 acoustic calibrator, generates a known SPL between 100 and 160 dB at a single frequency of 1000 Hz. The output of the optoelectronic amplifier was read on a B&K dual signal analyzer type 2032.

The *absolute sensitivity* of the FOLM system was measured at an SPL of 130 dB at 1000 Hz. The value obtained served as a reference sensitivity M_{SR} for the subsequent electrostatic actuator calibrations. The pistonphone sensitivity of microphone H18 was found to be 1.43 μV/Pa.

The *harmonic distortion* was measured by exciting the pistonphone at known SPLs (130, 140, 150, and 160 dB) at the fundamental frequency, 1000 Hz, and then measuring the

amplitudes of the second, third, and fourth harmonics. Higher harmonics were found negligible. The percent distortion d is defined as

$$d=\left(\frac{A_2^2+A_3^2+A_4^2}{A_1^2+A_2^2+A_3^2+A_4^2}\right)^{1/2}\times 100,$$

where A_i is the amplitude of the ith harmonic. The harmonic amplitudes were corrected for noise by the procedure described below [see Eq. (14)]. The measured distortion was found to be 0.44% at 150 dB and 1.4% at 160 dB.

B. Electrostatic actuator calibration

The electrostatic actuator[14] is a long established calibration method and is used today to calibrate commercial microphones. A fixed electrode is positioned near the microphone membrane. An applied voltage, an ac voltage superimposed upon a dc polarization voltage, generates an electrostatic pressure which excites the membrane at the frequency of the ac voltage. The magnitude of the electrostatic pressure is

$$p_{ea}=\epsilon_0 V_{ac}V_{dc}/h^2, \tag{13}$$

where ϵ_o is the dielectric permittivity of air, V_{ac} and V_{dc} the applied ac rms and dc voltages, and h the membrane–electrode gap. The advantages of the method are (1) adaptability to elevated temperatures and (2) excitation level independent of frequency and temperature, if the gap h can be maintained independent of temperature. The primary disadvantage is the low excitation level, which here requires special measures to obtain an acceptable signal-to-noise ratio.

The actuator electrode, a thick disk made of Inconel 601, contains three threaded holes, each seating a pin assembly. The latter consists of a set screw with an axial hole, into which a fused-quartz pin is bonded. The set screw permits adjustment of the gap, nominally 200 μm (0.008 in.), and the fused-quartz pin is intended to maintain a constant gap because of its low thermal-expansion coefficient. The electrode is positioned on the microphone weld ring (see Fig. 1) and contains a small hole on the top to accommodate a lead wire.

As indicated in Fig. 8(b) the microphone is mounted on a table made of Inconel 625, which contains a slot to secure the microphone by means of a tightening nut on its external threads. The optical fiber passes through a hole in the oven floor, packed with aluminum oxide wool. The lead to the actuator electrode is a 508-μm (0.02 in.) nichrome wire, insulated with thermocouple beads and Nextel™ (Al_2O_3) cloth. It is screwed to a ceramic standoff (not shown) mounted on the table, from which the end of a small loop is placed in the hole on the top of the actuator electrode. The table, cartridge, and membrane are earth-grounded by means of a similar nichrome lead. With nominal values V_{dc}=800 V, V_{ac}=60 V rms, and h=200 μm, an excitation level of 114 dB is achieved.

The supporting electronics incorporates features needed to satisfy several special measurement requirements. Because of the low output signal generated by the weak electrostatic excitation, the signal analyzer was operated in the "zoom" mode to reduce the noise contained in the excitation band. Typically a frequency resolution Δf of 0.5 or 0.25 Hz was selected, even 0.125 Hz on rare occasions. This required comparable frequency stability on the part of the oscillator, which here proved stable to within 0.1 Hz, even at excitation frequencies exceeding 100 kHz. Further, at 538 °C the air was disposed to electrical discharge at a polarization voltage of 800 V. This was indicated by the overload light on the power amplifier. Consequently, the polarization voltage supply was made adjustable, providing 0–800 V dc in 200-V steps. Finally, because the B&K signal analyzer was limited to a frequency response of 25.6 kHz, an alternative data-acquisition system, based on a portable computer and Analogic 6400 waveform digitizer, was used for measurements at higher frequencies. Although the absence of a true zoom capability prevented microphone calibration within the passband, the alternative system provided data in the vicinity of the membrane resonance frequency (as high as 140 kHz).

When the polarization voltage V_{dc} is set equal to zero, the output signal should vanish according to Eq. (13). This is a good test to insure that the output signal is truly due to mechanical motion of the membrane and not radiative pickup, as may be caused by faulty grounding or inadvertent ohmic contact between the electrode and membrane; it was performed prior to every frequency response calibration.

The first step in the *frequency response* calibration was to determine the electrostatic pressure from the response to the electrostatic excitation at 1000 Hz:

$$p_{ea}=M_{SR}V_{oR},$$

where M_{SR} is the known sensitivity from the pistonphone calibration at 1000 Hz and V_{oR} the measured output voltage. The frequency response calibration is based on the assumption that p_{ea} remains constant with frequency and temperature. Then M_S could be determined from the output voltage at any subsequent frequency and temperature.

The frequency response was measured over the range 10 Hz–25.6 kHz in discrete steps. For each measurement of the output voltage V_f at frequency f, the background noise voltages were simultaneously measured in the two adjacent frequency bands. Assuming the noise voltage V_n to be the mean of the two adjacent band voltages, we evaluated the true signal voltage rms V_o' to be

$$V_o'=\sqrt{(V_f^2-V_n^2)}. \tag{14}$$

Then the FOLM system sensitivity was simply p_{ea}/V_o'. With the narrow frequency resolution afforded by the zoom capability, the signal-to-noise ratio ranged from 6 to 20 dB. At 538 °C the same procedure was followed. Here the polarization voltage usually had to be reduced to 600 V, or sometimes 400 V, to prevent arcing, in which case the electrostatic pressure was corrected per Eq. (13).

The frequency response of microphone H18 at ambient temperature and 538 °C is shown in Fig. 9. The temperature variation of the sensitivity is seen to lie within 2 dB over the passband. The resonance frequency of the membrane surprisingly shifts upward from 70.5 to 71.0 kHz with a change from low to high temperature. The stiffening of the membrane is believed attributable to the onset of devitrification of

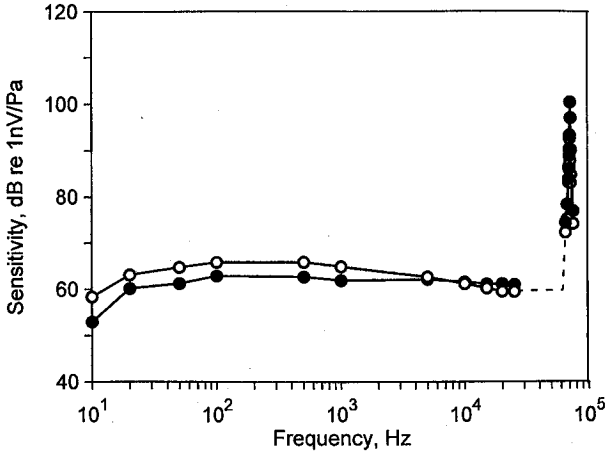

FIG. 9. Frequency response calibration of microphone H18 by the electrostatic actuator at ambient temperature (open circles) and 538 °C (filled circles). The excitation sound-pressure level is 114 dB. The dashed line represents the region not covered by the measurements.

the quartz layer. Monitoring the resonance frequency permitted us to track the membrane tension through Eqs. (2)–(4).

C. Background noise measurement

The setup shown in Fig. 8(b), with the electrostatic excitation disconnected, was used to measure the background noise. The noise is typically 22 μV within a 32-Hz band, corresponding to a sound pressure $V_n/M_S = 22/(1.43 \cdot \sqrt{32}) = 2.72$ Pa (102.7 dB) per $\sqrt{\text{Hz}}$. The spectrum at 538 °C shows slightly lower noise due to a reduction in optical power. Table II reveals that the listed theoretical noise sources account for about 80% of the experimental noise. The membrane radiation noise increases with temperature, as expected, but remains insignificant at 538 °C. However, it could become substantial in a 1093 °C FOLM system. A $1/f$ noise component appears at frequencies below 500 Hz.

D. Optical power meter measurement

Measurement of the optical transmission through the FOLM optical system provided a means of monitoring the condition of the optical fibers and the membrane mirror, especially at elevated temperatures. For this purpose a converter box was built, containing an LED and coupler as in the optoelectronic amplifier (Fig. 3), but the fiber to port 3 was directed to an SMA bulkhead connector to which the optical power meter was connected. An optical power measurement, performed with a Newport model 840 at a wavelength of 850 nm, accompanied every frequency response calibration. Results are shown in the next section.

E. Microphone stability with temperature cycling

The ability of the FOLM system to stabilize with repeated cycling to elevated temperatures was targeted as one of the most important specifications. With the setup shown in Fig. 8(b), a set of measurements at ambient temperature was followed by a set at 538 °C. After the microphone was allowed to soak at 538 °C for three hours, the high-temperature measurements proceeded, prolonging the soak for about an-

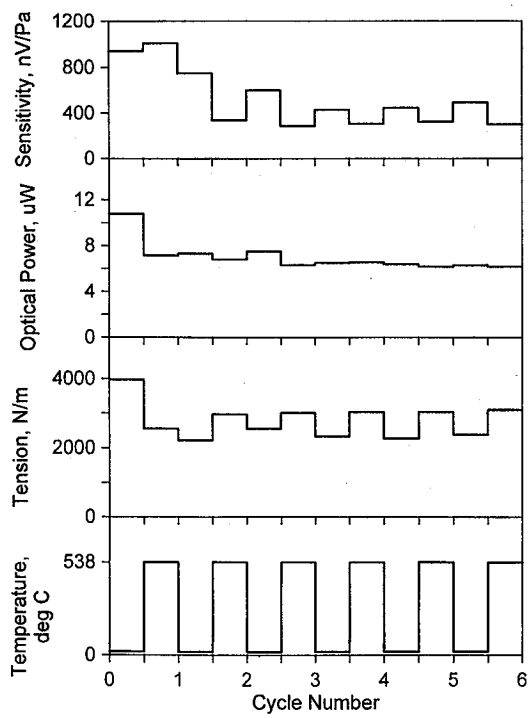

FIG. 10. Temperature cycling summary for microphone H15. From top: FOLM system sensitivity M_S, optical power P_t to the photodiode, membrane tension T, and temperature cycling profile.

other hour. A data set comprised the frequency response (including the membrane resonance frequency), background noise, and optical power transmission. An ambient temperature-elevated temperature cycle was completed in one day, after which the oven was turned off and permitted to cool to ambient temperature overnight.

A summary of the temperature cycling behavior is shown for microphone H15 in Fig. 10. This microphone is selected because it was cycled six times, the maximum number for any of the microphones. The temperature profiles at the bottom of the figure depict the cycling sequence and not the time history, for the soak time lasted approximately 4 h. The microphone sensitivity (at 1000 Hz) drops significantly after the first cycle but stabilizes after the third cycle, showing only low-to-high temperature variation. The optical power (at 850 nm) shows a large loss only after the first cycle, but stabilizes nicely thereafter. The membrane tension, derived from the resonance frequency, likewise shows an initial loss followed by stabilization with some low-to-high temperature variation. The resonance frequency during the sixth cycle varied from 43 kHz at 20 °C to 49 kHz at 538 °C, contrary to expected behavior as explained earlier. The cycling profiles shown here were found repeatable over many other microphones. The loss of optical power and sensitivity are believed due to a shift in fiber position relative to the mirror. Dissection of several microphones revealed no deterioration of the mirror or fibers. In the alternative optical fiber concept, using the seven element array, it was learned that temperature cycling caused the fibers to shift relative to one another and thus eroded the sensitivity. For this reason the seven element array was abandoned.

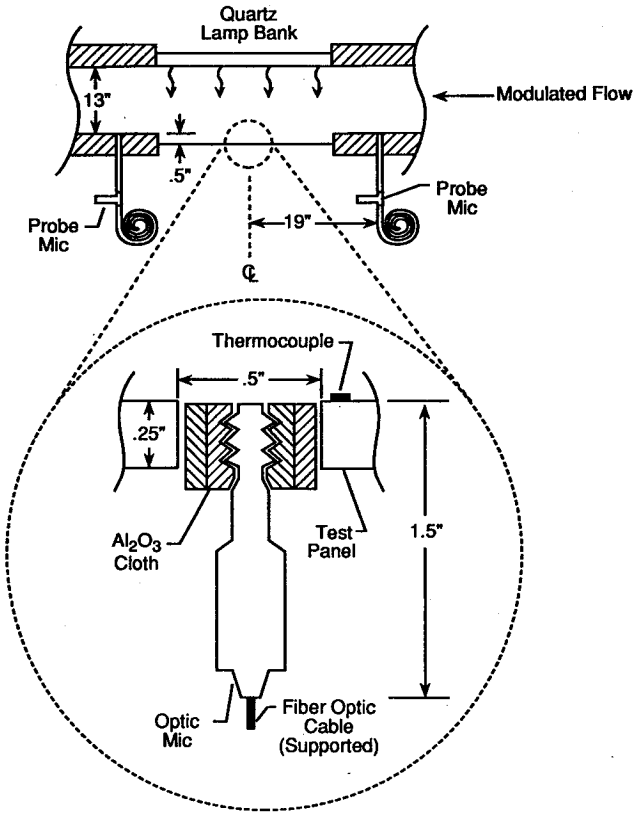

FIG. 11. Schematic diagram of the installation of the probe microphones and fiber-optic microphone in the wall of the TAFA test section.

V. FIELD TESTING OF THE FOLM SYSTEM

A. TAFA facility

The Thermal Acoustic Fatigue Apparatus (TAFA) facility at Langley Research Center is a grazing incidence, high-intensity noise apparatus with the capability of generating overall sound-pressure levels (OASPL) from 125 to 168 dB, both sinusoidal and random, in the frequency range of 40–500 Hz. Figure 11 shows a schematic of the facility test section. The noise source (not shown) is composed of two 30 000-W acoustic modulators driven by filtered pressurized air. The sound is coupled at grazing incidence to the 1.829 m×1.829 m (6 ft×6 ft) test section by an exponential horn (not shown) with a 27-Hz low-frequency cutoff. Test panels or plates can be mounted in one movable wall of the test section. On the opposite wall, a heat bank of ten high-intensity lamp fixtures with six 6000-W quartz lamps in each is located behind a 0.025-m (1 in.) thick quartz window. This system is used to obtain heating flux densities up to 510 kW/m^2 [44 $Btu/(ft^2\ s)$] on the test panel surface. Both the test panel wall and the heat bank wall are water cooled and the lamp bank is both air and water cooled. For more details see Ref. 15.

For normal operation two probe microphones are used: one is located at 0.483 m (19 in.) upstream and the other located at 0.483 m (19 in.) downstream of the vertical centerline of the test section, as shown in Fig. 11. These are specially configured to measure the noise levels near the test panel during high-temperature operation. The microphones themselves are positioned 0.457 m (18 in.) behind the rear surface of the test wall in a "Tee" of a 0.0064-m (1/4 in.) diameter pipe penetrating the test section. A 15.24-m (50 ft) length of 0.0064-m (1/4 in.) tubing behind each microphone is used to eliminate reflective tube resonances. These microphones are calibrated using a noise driver as a source to drive noise down a 0.0254-m (1 in.) diameter pipe. The end of the 0.0064-m (1/4 in.) probe pipe normally penetrating the test section wall is sealed inside one side of the 0.0254-m (1 in.) diameter pipe and a calibrated microphone is sealed inside directly opposite it. The output of the probe microphone is adjusted to equal the output of the calibrated microphone at 124 dB and 250 Hz. Experience has shown that the effects of thermal gradients inside the probe tube during high-temperature operations are negligible.

B. Fiber-optic microphone installation

The fiber-optic microphone was installed at the center position of a very stiff test panel as shown in Fig. 11. The panel was made of 0.0064-m (1/4 in.) thick steel with two 0.1016-m (4 in.) steel angle stiffeners attached to the rear surface. The 0.0127-m (1/2 in.) offset was acoustically negligible in the frequency range of interest. This arrangement provides the desired test conditions, temperatures up to 538 °C and sound-pressure levels up to 160 dB. The membrane end of the microphone cartridge was fitted into a high-temperature gasket, made of aluminum oxide cloth, and flush-mounted into the 0.0127-m (1/2 in.) hole in the panel. A thermocouple was installed on the test panel next to the membrane to monitor the temperature in the vicinity of the fiber-optic microphone. The optoelectronic amplifier was located in the TAFA control room and connected to the microphone with a 5.0-m (16.4 ft) long fiber extender. The fiber cable was supported by two poles, which stood adjacent to, but not in contact with, the test panel. This arrangement was successful in isolating the microphone and fiber cables from the substantial vibrations of the TAFA structure.

C. Data acquisition and analysis

Time series microphone data were first acquired using a spectrum analyzer for four overall sound-pressure levels (130, 140, 150, and 160 dB) and three temperature conditions (ambient and 268 and 538 °C). In each of the above, 10 s of data were recorded at a time resolution Δt of 1.22×10^{-4} s. The time series data were then postprocessed to determine the power spectral density (PSD) of the sound-pressure level. Each record was divided into contiguous 0.5-s blocks and a Hanning window was applied to each. A 4096-point transform was taken, yielding a frequency resolution of 2 Hz. Twenty PSDs were averaged to obtain the final results. The exception to the above was the acquisition and processing of the 160-dB data at 538 °C. 2 s of data were recorded in this case, allowing only four averages to be performed. Therefore the spectra shown in Sec. V D are not as smooth as the other cases.

D. Results

The following results correspond to a bandlimited input spectra to the TAFA noise generation system between 50 and

TABLE III. Overall sound-pressure levels (0–500 Hz) measured by the probe tube and fiber-optic microphones, and their difference, at three temperatures.

Nominal OASPL (dB)	Probe tube/FOLM/difference (dB)		
	Ambient	260 °C	538 °C
130	130.8/134.0/−3.2	129.4/137.0/−7.6	129.4/146.8/−17.4
140	139.5/141.7/−2.2	140.1/141.7/−1.6	139.2/147.6/−8.4
150	150.4/152.4/−2.0	150.0/150.5/−0.5	149.9/152.5/−2.6
160	160.0/162.3/−2.3	159.8/160.2/−0.4	159.8/160.9/−1.1

200 Hz. The overall levels from the probe tube and fiber-optic microphones, and their differences, were computed and are shown in Table III for the ambient and 268 and 538 °C temperatures. From this data, it is apparent that the noise floor of the fiber-optic microphone is somewhere between the 130 and 140 dB sound-pressure levels, depending on the temperature. Figure 12 shows the power spectral densities of the fiber-optic microphone at 538 °C for noise levels of 130, 140, 150, and 160 dB OASPL. The high-temperature, low-frequency background noise has the appearance of a $1/f$ component. Experience has shown that this effect anneals out after several thermal cycles. However, since the data were collected prior to repeated thermal cycling, the $1/f$ component did not have the opportunity to anneal out. Table III shows that the OASPL measured by the fiber-optic microphone are as much as 1–2.3 dB high for those tests where the background noise plays an insignificant role. The discrepancy is attributable to the fact that the probe microphone was not located at the same location as the fiber-optic microphone. Figure 13 shows a comparison between the power spectral densities of the fiber-optic microphone and the probe microphone at the 160 dB OASPL at 538 °C. It is seen from the data that the shapes of the spectra compare well. The spectra at ambient and 268 °C (not shown) compare equally well.

E. Discussion of field test

As is evident in Fig. 13, the fiber-optic microphone reproduced the spectral shape of the acoustic pressure measured by the probe microphone. The absolute power spectral densities, however, differ from those of the probe microphone, as indicated in Table III. At a sound-pressure level of 130 dB, the influence of the background noise in the fiber-optic microphone is evident, especially at 538 °C, where a prominent $1/f$ component appears. At the higher sound-pressure levels the $1/f$ component is less significant and the two measurements compare favorably in both shape and overall level. The ability of the microphone to reproduce the spectra at 160 dB reveals good microphone linearity at all temperatures, as is to be expected, for the microphone was designed to measure levels up to 190 dB. The limited bandwidth of the test (50–200 Hz) did not utilize the full frequency response capability of the microphone, for the membrane has a resonance frequency of about 70 kHz. A drawback was the unexpected sensitivity of the fiber-optic microphone to vibration (changes in optical intensity). The microphone has to be isolated from the vibration of the TAFA carriage for the test to be successful. The vibration sensitivity is thought to originate in the response to microbending by the multimode optical fibers, and will have to be addressed in further development of the microphone.

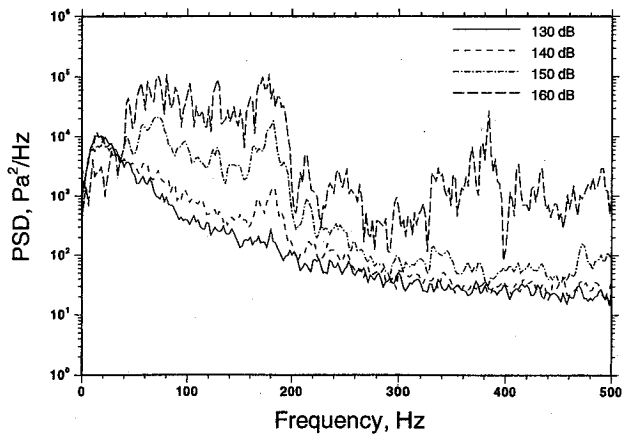

FIG. 12. Power spectral densities of the acoustic pressure measured by the fiber-optic lever microphone at 538 °C.

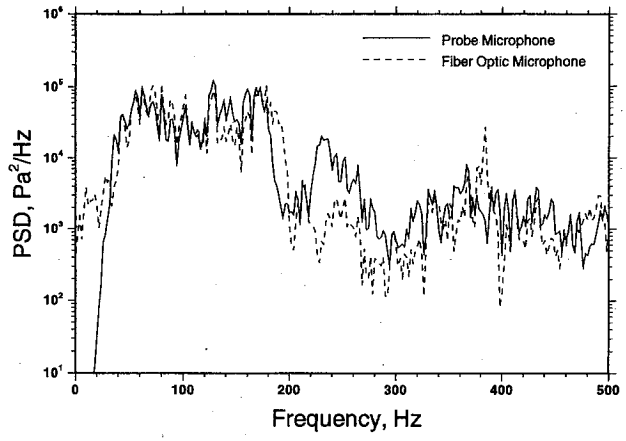

FIG. 13. Comparison of power spectral densities of acoustic pressure measured by the probe and fiber-optic microphones at 160 dB and 538 °C.

ACKNOWLEDGMENTS

The authors wish to thank the following Langley colleagues: W. E. Robbins and D. R. Barnes for designing and fabricating the microphone cartridges, K. D. Wright for designing the optoelectronic amplifier, and E. F. Daniels and G. A. Parker for assistance in conducting the TAFA field test. The work of two of the authors (F. W. C. and T. D. N.) was supported under Contracts No. NAS1-19505-9 and No. NAS1-18584-143, respectively.

[1] D. A. Berlincourt, D. R. Curran, and H. Jaffe, "Piezoelectric and piezomagnetic materials and their function in transducers," *Physical Acoustics*, edited by W. P. Mason (Academic, New York, 1966), Vol. IA.

[2] *Silicon Temperature Sensors and Pressure Sensors Data Book 1990/91* (Siemens AG, Munich, 1990).

[3] J. C. Schneider and R. K. Duke, "Phase II development of a 1093 °C (2000 °F) prototype microphone transducer," Technical Report AFFDL-TR-74-136, December 1974.

[4] J. A. Bucaro, N. Lagakos, J. H. Cole, and T. G. Giallorenzi, "Fiber optic acoustic transduction," *Physical Acoustics*, ed-

ited by W. P. Mason and R. N. Thurston (Academic, New York, 1982), Vol. XVI.
[5] *Condenser Microphones and Microphone Preamplifiers for Acoustic Measurements: Data Handbook* (Bruel & Kjaer Instruments, Naerum, Denmark, 1982).
[6] T. Parrott and W. Zorumski, "Sound transmission through a high-temperature acoustic probe tube," AIAA-90-3991-CP, 1990.
[7] G. He and F. W. Cuomo, "Dynamic response, detection limit, and dynamic range of fiber-optic lever sensors," J. Lightwave Technol. **9**, 1618–1625 (1991).
[8] W. Betteridge, *Nickel and Its Alloys* (Horwood, Chichester, England, 1984), p. 66.
[9] P. M. Morse and K. U. Ingard, *Theoretical Acoustics* (McGraw-Hill, New York, 1968), p. 211.
[10] A. Hu, F. W. Cuomo, and A. J. Zuckerwar, "Theoretical and experimental study of a fiber optic microphone," J. Acoust. Soc. Am. **91**, 3049–3056 (1992).
[11] G. He and F. W. Cuomo, "A light intensity function suitable for multimode fiber-optic sensors," J. Lightwave Technol. **9**, 545–551 (1991).
[12] T. G. Giallorenzi, J. A. Bucaro, A. Dandridge, G. H. Sigel, J. H. Cole, S. C. Rashleigh, and R. G. Priest, "Optical fiber sensor technology," IEEE J. Quantum Electron. **QE-18**, 626–665 (1982).
[13] G. He and F. W. Cuomo, "The analysis of noises in a fiber optic microphone," J. Acoust. Soc. Am. **92**, 2521–2526 (1992).
[14] G. Rasmussen, "The free field and pressure calibration of condenser microphones using electrostatic actuator," B&K Technical Review 2-1969.
[15] S. A. Clevenson and E. F. Daniels, "Capabilities of the thermal acoustic fatigue apparatus," NASA TM 104106, 1992.